

Isotope effect on hydrated electron relaxation dynamics studied with time-resolved liquid jet photoelectron spectroscopy

Madeline H. Elkins, Holly L. Williams, and Daniel M. Neumark

Citation: *The Journal of Chemical Physics* **144**, 184503 (2016); doi: 10.1063/1.4948546

View online: <http://dx.doi.org/10.1063/1.4948546>

View Table of Contents: <http://scitation.aip.org/content/aip/journal/jcp/144/18?ver=pdfcov>

Published by the **AIP Publishing**

Articles you may be interested in

[Excited state non-adiabatic dynamics of N-methylpyrrole: A time-resolved photoelectron spectroscopy and quantum dynamics study](#)

J. Chem. Phys. **144**, 014309 (2016); 10.1063/1.4938423

[Excited state dynamics in SO₂. I. Bound state relaxation studied by time-resolved photoelectron-photoion coincidence spectroscopy](#)

J. Chem. Phys. **140**, 204301 (2014); 10.1063/1.4875035

[C 6 – electronic relaxation dynamics probed via time-resolved photoelectron imaging](#)

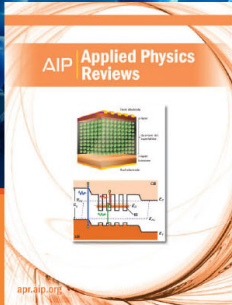
J. Chem. Phys. **121**, 3515 (2004); 10.1063/1.1769368

[Dynamics of excited-state proton transfer systems via time-resolved photoelectron spectroscopy](#)

J. Chem. Phys. **114**, 2519 (2001); 10.1063/1.1345876

[The nonradiative decay of the allyl radical excited B 2 A 1 state studied by picosecond time-resolved photoelectron spectroscopy](#)

J. Chem. Phys. **107**, 8197 (1997); 10.1063/1.475121



NEW Special Topic Sections

NOW ONLINE
Lithium Niobate Properties and Applications:
Reviews of Emerging Trends

AIP | Applied Physics
Reviews

Isotope effect on hydrated electron relaxation dynamics studied with time-resolved liquid jet photoelectron spectroscopy

Madeline H. Elkins,^{1,a)} Holly L. Williams,¹ and Daniel M. Neumark^{1,2,b)}

¹Department of Chemistry, University of California, Berkeley, California 94720, USA

²Chemical Sciences Division, Lawrence Berkeley National Laboratory, Berkeley, California 94720, USA

(Received 28 February 2016; accepted 20 April 2016; published online 10 May 2016)

The excited state relaxation dynamics of the solvated electron in H₂O and D₂O are investigated using time-resolved photoelectron spectroscopy in a liquid microjet. The data show that the initial excited state decays on a time scale of 75 ± 12 fs in H₂O and 102 ± 8 fs in D₂O, followed by slower relaxation on time scales of 400 ± 70 fs and 390 ± 70 fs that are isotopically invariant within the precision of our measurements. Based on the time evolution of the transient signals, the faster and slower time constants are assigned to $p \rightarrow s$ internal conversion (IC) of the hydrated electron and relaxation on the ground electronic state, respectively. This assignment is consistent with the non-adiabatic mechanism for relaxation of the hydrated electron and yields an isotope effect of 1.4 ± 0.2 for IC of the hydrated electron. *Published by AIP Publishing.* [<http://dx.doi.org/10.1063/1.4948546>]

I. INTRODUCTION

Hydrated electrons were first identified in 1962 by their absorption spectrum at 720 nm.¹ Since then, electrons solvated in water and other solvents have been implicated in fields as far reaching as the photo-induced chemistry of DNA²⁻⁴ to the nature of the Coulomb explosion following the addition of sodium metal to water,⁵ and even to the ultrafast photophysics of liquid nanodroplets.⁶ Because the solvated electron lacks internal degrees of freedom, it can be thought of as a model solute for studying solvation phenomena. The coupling of the electronic degree of freedom of an excited hydrated electron to the various solvent nuclear modes is a fundamental example of intrinsically non-adiabatic dynamics in solution. These dynamics are of particular interest given that electronically excited hydrated electrons are more reactive than those in their ground state.⁷ In this work, the effect of isotopic substitution on the excited state dynamics of the hydrated electron is investigated using time-resolved photoelectron spectroscopy (TRPES) on liquid jets of H₂O and D₂O.

Many aspects of the hydrated electron, e_{aq}^- , are under investigation. The generally accepted picture of e_{aq}^- is that it occupies a quasi-spherical cavity in water with an approximate radius of 2.5 Å,^{8,9} although alternative structures have been proposed over the years.¹⁰⁻¹³ The absorption spectrum of e_{aq}^- exhibits a broad band with a maximum at 720 nm, which has been assigned to transitions from the “s-like” ground state to a non-degenerate manifold of “p-like” excited states within the solvent cavity.^{9,14,15} The time-resolved dynamics of hydrated electrons are also of considerable interest, as evidenced by the many experimental and theoretical investigations focused on understanding of how equilibrated hydrated electrons are formed by direct ionization of water molecules¹⁶ or by to charge-transfer-to-solvent (CTTS) excitation of aqueous

anions.¹⁷ This body of work is discussed in reviews by Bradforth¹⁸ and Rossky.¹⁹

The present work builds upon a wealth of previous experiments aimed at mapping out the dynamics of e_{aq}^- subsequent to excitation of the $s \rightarrow p$ transition near 720 nm. Of particular interest is a set of transient absorption (TA) experiments involving a three laser pulse excitation/detection scheme.²⁰⁻²⁵ The first pulse generates electrons by ionization of water or by CTTS excitation in the ultraviolet and allowed to equilibrate. The $s \rightarrow p$ transition is then excited with a second fs laser pulse, and the resulting dynamics are monitored by transient absorption with a (third) broadband probe pulse. In these experiments, three lifetimes were measured: <100 fs, 200-400 fs, and 1.1 ps. Similar results were also obtained in D₂O and yielded an isotope effect for the fast lifetime of 1.1-1.5; however, no measurable isotope effect was observed for the 200-400 fs transient.^{20,24,25}

The importance of isotope effects derives from long-standing discussions on the interpretation of the time scales in TA subsequent to excitation of the $s \rightarrow p$ transition.^{12,19,26-30} Two general relaxation mechanisms for the photo-excited p -state have been proposed, the “adiabatic” and “non-adiabatic” mechanisms.^{19,20} In the adiabatic mechanism, the fastest (<100 fs) lifetime is assigned to solvent relaxation on the excited state, τ_p . The 200-400 fs lifetime is assigned to internal conversion (IC) from the excited state to the ground state, τ_{IC} , and the 1.1 ps lifetime corresponds to solvent relaxation on the ground state, τ_s . In the “non-adiabatic” mechanism,^{24,31} the fastest lifetime is assigned to IC, and the two longer lifetimes are assigned to relaxation on the ground state.

Since assignment of the transients in the TA experiments is ambiguous, it is desirable to devise an independent measure of the IC rate and thereby distinguish between these two mechanisms. Novel experimental and theoretical approaches have addressed this issue. Scavenging experiments by Barbara³² suggested a lifetime of 300 fs, in support of the adiabatic model. Recent polarization anisotropy experiments

^{a)}Present address: Department of Chemistry, Princeton University, Princeton, NJ 08544, USA.

^{b)}dneumark@berkeley.edu

by Loh,³³ on the other hand, yielded a p -state lifetime of 79 fs, supporting the non-adiabatic mechanism. Mixed quantum-classical molecular dynamics (QC-MD) calculations have generally found p -state lifetimes of several hundred fs,^{26,27,34,35} although the incorporation of additional quantum effects drops this value to as low as 122 fs.³⁶ A Golden Rule calculation yields an IC lifetime of <100 fs but suggests that the effective lifetime measured experimentally is around 300 fs.²⁹

Isotope effects provide an important perspective on the hydration dynamics of e_{aq}^- . In addition to being seen in TA experiments, they have been observed in the fluorescence quantum yield of e_{aq}^- ,³⁷ in time-resolved polarization anisotropy experiments following multiphoton ionization of liquid water³³ and in excited state lifetimes in water cluster anions as measured by time-resolved photoelectron spectroscopy.^{38–40} In theoretical work, the mixed quantum/classical calculations by Nitzan³⁴ and Rossky²⁶ found IC lifetimes in D₂O to be longer by factors of 3.6 and ~2, respectively, relative to H₂O; this effect was attributed to the fastest nuclear velocities in D₂O being slower than those in H₂O by a factor of $\sqrt{2}$, leading to reduced electronic-nuclear coupling. A continuum model proposed by Zharikov and Fischer⁴¹ predicts an isotope effect of $\sqrt{2}$ on the IC rate. These results suggest that an experimental time scale that does not exhibit a strong isotope effect, such as the 200–400 fs time scale seen in the TA experiments, arises from something other than IC. However, Rossky, Schwartz, and co-workers^{35,36,42} have shown that it is important to consider quantum decoherence in mixed QC-MD simulations of e_{aq}^- and that, depending on how these effects are incorporated, the calculated isotope effect on the IC rate can decrease or disappear. Isotope effects have also been shown to be important in the excited state hydration dynamics of e_{aq}^- .⁴³

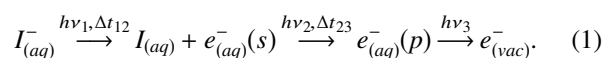
Additional insights into hydrated electron dynamics are obtained from time-resolved photoelectron spectroscopy experiments on gas phase water cluster anions^{38–40,44,45} and solvated electrons in liquid microjets.^{46–52} In the cluster experiments, (H₂O)_n⁻ and (D₂O)_n⁻ clusters as large as n = 200 were generated and studied using TRPES.^{38–40,44,53,54} These experiments showed a clear separation between the s and p states, allowing for conclusive identification of the internal conversion lifetime. This lifetime was measured as a function of cluster size and then extrapolated to a bulk value of 63 fs in water and 160 fs in D₂O.⁴⁰ The extrapolated lifetimes were interpreted as supporting the non-adiabatic mechanism in bulk water, an interpretation that relies on the validity of extrapolating cluster dynamics to those in bulk water.

In order to bridge the gap between experiments on water cluster anions and those in bulk water, photoelectron spectroscopy experiments on hydrated electrons in liquid water microjets⁵⁵ have been carried out in our laboratory^{46,51} and elsewhere.^{47–49,56–58} Three-pulse TRPES experiments on electrons in a liquid water jet yielded features with decay times of 75 and 400 fs that were assigned, based on their temporal evolution and energy separation, to the IC lifetime and relaxation time on the ground state, respectively. This assignment is again in support of the non-adiabatic mechanism.⁵¹

Here, we report on three-pulse TRPES experiments on e_{aq}^- in liquid jets of D₂O. These experiments have multiple

objectives. First, if the fastest decay time is slower in D₂O than in H₂O, it should be possible to better characterize the time-evolution of the transient signals in D₂O and test their previous assignments. Second, measurements of the dynamics in the H₂O and D₂O jets will provide an important point of comparison with previous work using TA spectroscopy of bulk water and TRPES of water cluster anions. Finally, comparison to theoretical work can provide insight into understanding how, and if, internal conversion depends on isotope effects.

The experiment is conducted following the excitation scheme in Eq. (1). Solvated electrons in water and deuterated water are generated by charge-transfer-to-solvent (CTTS) excitation of iodide with a first photon.¹⁸ The nascent photoelectrons are allowed to equilibrate with the solution, and after a 200 ps delay, a second photon excites the $s \rightarrow p$ absorption band of the solvated electron. At a variable delay, a third photon detaches the excess electron to vacuum, and the ensuing dynamics are monitored by measuring the binding energy of the electron as a function of delay Δt_{23} ,



We find that photoelectrons signals ejected with the highest kinetic energy decay on time scales of 75 ± 12 fs for water and 102 ± 8 fs for deuterated water, corresponding to an isotope shift 1.4 ± 0.2 . Slower electrons exhibit a second decay time of 390–400 fs that shows no measurable isotope shift. Based on the time evolution of the transient signals, the fast and slow decays are assigned to IC and subsequent solvent relaxation, respectively. Taken with earlier results in our laboratory and elsewhere, these results offer additional support for the non-adiabatic mechanism of hydrated electron relaxation and show that isotope effects do play a significant role in internal conversion.

II. METHODS

The liquid microjet photoelectron spectrometer used for these experiments has been described previously.⁵² Briefly, a solution of potassium iodide (100 mM, Fischer) in water (18 M Ω , Millipore) or deuterium oxide (99.98% Cambridge Isotope Laboratories) is injected at high backing pressure, 80–130 atm, through a 20 μ m fused silica capillary into vacuum. The flow rate is held at 0.33 ml/min for both water and heavy water, resulting in a jet velocity of ~13 m/s. The liquid is then crossed with a series of femtosecond laser pulses following the excitation scheme in Eq. (1). The crossing point is 1 mm downstream of the capillary tip, where the temperature is estimated to be ~280 K as adapted from the temperature gradient model of Smith *et al.*⁵⁹ in our previous work.⁴⁶

Photoelectrons ejected into vacuum are sampled through a 900 μ m skimmer. Typical values of kinetic energy are 1–3 eV, corresponding to an escape depth of a few nanometers.^{56,57,60,61} The photodetached electrons are energy-analyzed with a magnetic bottle consisting of a 1.1 T SmCo magnet and a 10 G solenoid. This technique results in greatly increased photoelectron collection efficiency over field-free time of flight, up to a theoretical solid angle of 2π steradians.^{48,62}

The photoelectrons are detected by a chevron-mounted pair of microchannel plates coupled to a phosphor screen that is used to optimize alignment of the magnetic bottle and liquid jet. Data are recorded in the form of the capacitively coupled current from the phosphor screen as a function of time between the laser interaction with the jet and arrival at the detector. This time-of-flight is converted to electron kinetic energy (eKE), and the photoelectron intensity is scaled with the appropriate Jacobian transformation (t^{-3}). Accounting for the resolution of the spectrometer, laser bandwidth, and uncertainty in the measured streaming potential, the energy resolution of the instrument is ~ 50 meV. Calibration of the instrument and measurement of the streaming potential⁵⁰ are as described in our previous paper.⁶³

Ultrafast pulses are generated from the 800 nm output from a commercial ultrafast system (Spectra Physics Spitfire, 2.2 W, <75 fs). Approximately half the output is directed into an optical parametric amplifier (Light Conversion TOPAS). The second harmonic of the sum of the signal and pump is used to generate the tunable ultraviolet wavelength used for CTTS excitation (240 nm, $h\nu_1$). The rest of the output from the femtosecond system is either used directly to form $h\nu_2$ (800 nm) or tripled to form the probe (266 nm, $h\nu_3$). Improvements to the optical layout since our previous work have allowed for a shorter cross-correlation at the chamber, 65 fs (Gaussian width).

III. RESULTS

Following the excitation scheme in Eq. (1), a UV pulse at 240 nm, $h\nu_1$, is used to generate solvated electrons via CTTS

excitation. After a 200 ps delay, the electrons are excited by $h\nu_2$ at 800 nm and detached to vacuum with $h\nu_3$ at 266 nm. Data are recorded at pump-probe delays Δt_{23} from -1 ps to 10 ps. The TRPE spectrum as a function of Δt_{23} for D_2O is shown in Figure 1(a). The spectrum in Fig. 1(a) is shown with contributions from each individual UV beam subtracted, $(h\nu_1 + h\nu_2 + h\nu_3) - h\nu_1 - h\nu_3$; both $h\nu_1$ and $h\nu_3$ contribute static, single color photoelectron intensity that is treated as background. Fig. 1(a) shows that there is a transient centered around 2.6 eV that decays by 100-150 fs. Near 1.2 eV, at the top of the largest feature in the spectrum, we observe a dip near $\Delta t_{23} = 0$ that fills in on a time scale of several hundred fs. Less apparent is a transient feature around 2 eV that decays on a time scale similar to the recovery of the feature at 1.2 eV.

Another perspective on these data is provided by Figs. 1(b) and 1(c), which show the spectra with and without $h\nu_2$, $(h\nu_1 + h\nu_2 + h\nu_3) - (h\nu_1 + h\nu_3)$, in H_2O and D_2O , respectively. These difference spectra show how $h\nu_2$, which excites the $s \rightarrow p$ transition, changes the spectrum. Moreover, they emphasize how the overall shape of the transient changes with time above 2 eV. The signal above 2.6 eV exhibits a shoulder that decays on a time scale of <100 fs, leaving a more slowly decaying transient from 1.9 to 2.3 eV that decays and shifts toward lower eKE on a time scale of several hundred fs.

The blue, red, and green shaded regions in Fig. 1(a) represent kinetic energy lanes with distinct temporal evolution. Fig. 2(a) shows normalized plots of the integrated intensity in these three regions for D_2O ; the energy ranges are given in the legend. The specific choice of electron kinetic energy intervals

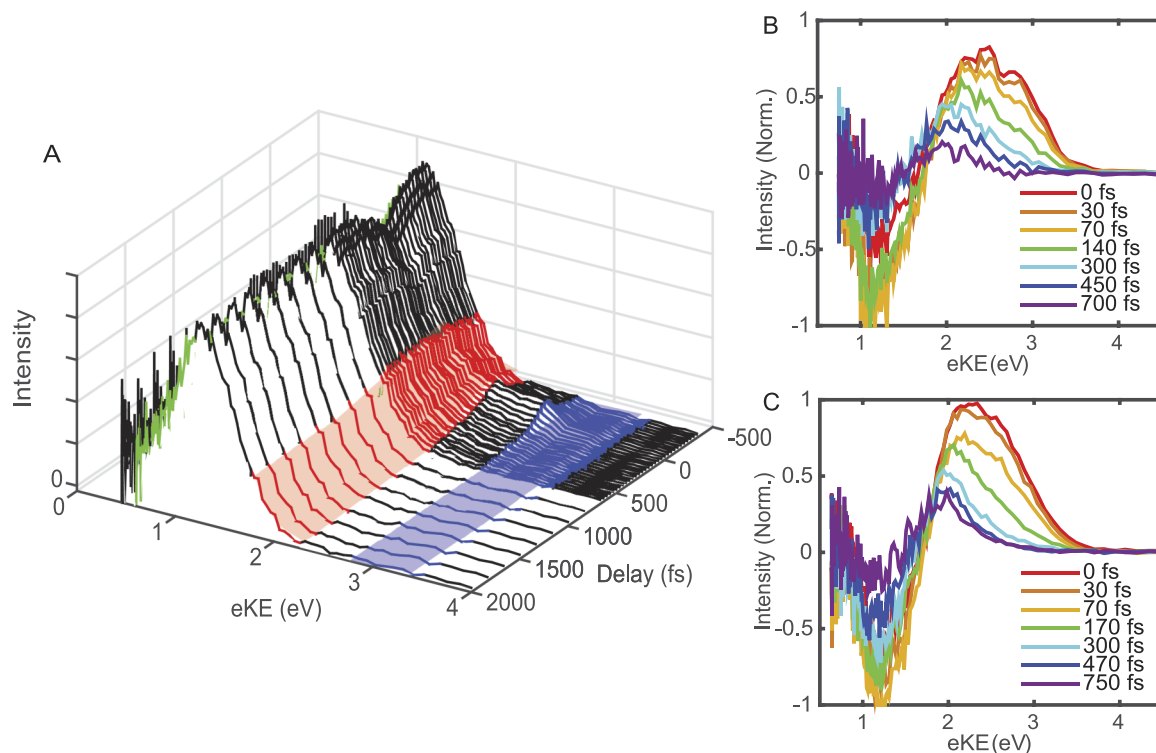


FIG. 1. Time-resolved (TR) data for hydrated electrons in H_2O and D_2O using two subtraction methods. (a) TRPE spectra for D_2O showing the photoelectron kinetic energy (eKE) distribution plotted vs. Δt_{23} (see Eq. (1)) with each ultraviolet one-color contribution subtracted, $(h\nu_1 + h\nu_2 + h\nu_3) - h\nu_1 - h\nu_3$. (b) and (c) PE at selected delay times with and without IR pump beam in H_2O and D_2O , respectively, $h\nu_2$, $(h\nu_1 + h\nu_2 + h\nu_3) - (h\nu_1 + h\nu_3)$.

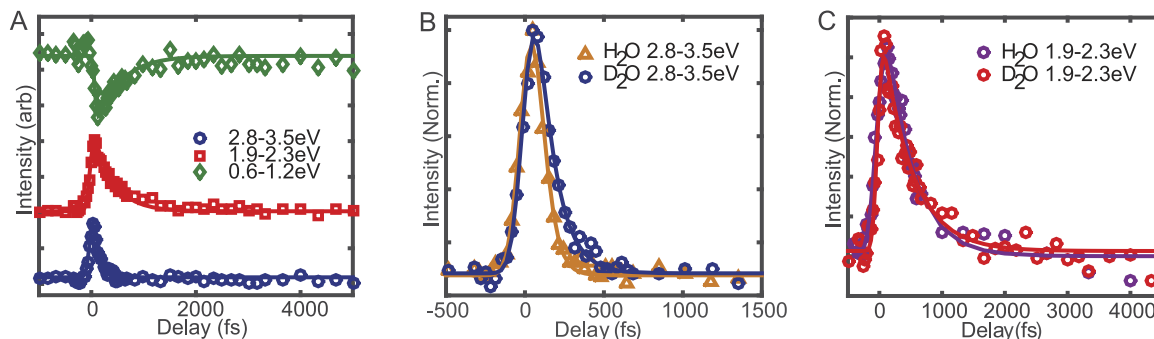


FIG. 2. Integration of the TR spectra in selected energy lanes for both solvents. Shown in Panel (a) are the three regions of interest for D_2O ; energy lanes for the blue, red, and green ranges are given in the legend. (b) and (c) Comparison of blue (b) and red (c) lanes in H_2O and D_2O . Data are shown as symbols, and curves are fits as discussed in Section IV.

for the three regions is discussed in Section IV. The decay of signal in the blue lane, the highest eKE signal, spanning 2.8-3.5 eV is complete within the first 100 fs. The red lane signal, covering 1.9-2.3 eV, decays within several hundred fs. Signal in the green lane, from 0.6-1.2 eV, is depleted but then recovers on a time scale similar to that of the red lane decay time. These results are typical for both isotopes.

The effects of isotopic substitution in are shown in Figs. 2(b) and 2(c). Fig. 2(a) shows that the decay of the blue lane signal in H_2O , the gold triangles, is noticeably faster than the decay of this signal in D_2O , the blue circles. The decay dynamics in the red lane are somewhat less obvious. A fit to the integrated intensity in this region will be affected by the dynamics from any overlapping features. This effect was observed in water, D_2O , and in methanol.⁵² Shown in Fig. 2(c) is a comparison of the red lane signals in water and D_2O ; there is no obvious change in the decay times. Details of the fitting procedure used in Fig. 2 are described in Section IV.

Without further interpretation, we can understand the dynamics in Figs. 1 and 2 in the following manner. The initial dip around 1.2 eV kinetic energy represents the pump-induced depletion of the initial state. In water and heavy water, this feature is identified as a depletion of the ground state photoelectron intensity. This assignment is made based upon the known vertical binding energy (VBE) of the hydrated electron, 3.4 eV,⁴⁸⁻⁵⁰ as characterized by the peak of the electron kinetic energy distribution, $h\nu_3 - eKE_{peak} = VBE$. The decay of the blue and red signals reflects the relaxation of the population excited after the pump pulse as the equilibrated ground state of e_{aq}^- is repopulated. These features have been discussed previously in water⁵¹ and in methanol,⁵² where they were interpreted as internal conversion and ground state relaxation, respectively. The new results presented here include a more detailed spectral analysis of the TRPE data, discussed in Sec. IV, and consideration of the isotope effect on the internal conversion dynamics, Sec. V.

IV. ANALYSIS

In order to gain a more quantitative understanding of the time resolved data, two general data analysis methods are employed, Global Lifetime Analysis (GLA)^{64,65} and lane integration in which the electron signal within selected energy

window is integrated and followed as a function of time. The latter presents a simpler method of data analysis with few fit parameters, but can be problematic when multiple features overlap in the same spectral region. Global fitting techniques such as GLA have proven to be particularly advantageous for decomposing the spectral contributions from overlapping features in congested spectra and have been used effectively in analyzing TRPE spectra.⁶⁶⁻⁶⁸ GLA allows for a spectral decomposition of the time-evolving features, but the method suffers in the presence of dynamic spectral shifts, which are typical of solvent relaxation processes.⁶⁹ Two sets of spectra extracted from global fitting are presented: first, the decay associated spectrum/spectra (DAS) for each kinetic component and, second, a reconstructed spectrum for the feature of interest. The DAS is the amplitude for each kinetic component as a function of kinetic energy and is an output from the fit. The extracted spectra are calculated from the DAS using a particular kinetic model. Here, both methods provide complementary information on the TR data.

As discussed previously,⁵² inherent in GLA is the assumption that the data consist of a sum of spectral components, each of which is separable into two parts: the spectrum of the component, $S_j(eKE)$, which depends only on kinetic energy, and a kinetics term, $S_j(\Delta t)$, which depends only on pump-probe delay. This sum is expressed mathematically in Eq. (2a), in which each component in the sum is scaled by the relative photodetachment cross section, σ_r , and where the sum is indexed by the number of spectral components j . In addition, the kinetics term is assumed to take the form of sums of mono-exponentials (ex. $S(\Delta t) = Ae^{-k_1t} + Be^{-k_2t}$). If both assumptions are true, the data can be represented as a sum of exponentials scaled by a constant which depends on energy, called the decay associated spectrum (DAS),⁶⁴ and indexed by the time constants $\tau_i = 1/k_i$, Eq. (2b),

$$S(eKE, \Delta t) = \sum_{j=1}^n \sigma_{r,j} S_j(eKE) \times S_j \Delta t, \quad (2a)$$

$$S(eKE, \Delta t) = \sum_{i=1}^n DAS_{\tau_i}(eKE) \times [e^{-z/\tau_i} * L(z - \Delta t)]. \quad (2b)$$

The fit, residuals, and decay associated spectra generated from global lifetime analysis of the D_2O time-resolved data are shown in Figs. 3(b)-3(d). In D_2O , two kinetic components

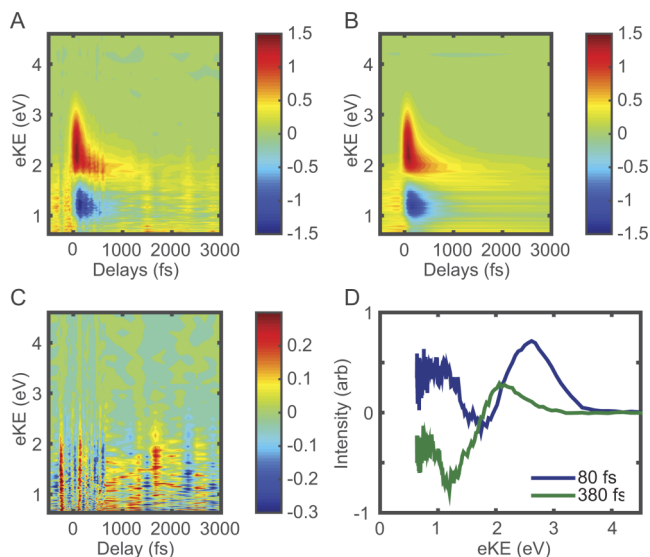


FIG. 3. Global lifetime analysis of D₂O data. (a) Raw TR data, (b) Global fit to Eq. (2b), (c) Residuals, and (d) Decay associated spectra.

are found to fit the spectra, 80 ± 30 fs and 380 ± 90 fs. DAS features that are positive going are associated with features that decay and features that are negative going are associated with features that rise. DAS_{80} shows two peaks: one centered at 0.9 eV eKE and one at 2.5 eV eKE. The peak at 0.9 eV is readily identifiable as the ground state spectrum from prior work.⁵⁰ DAS_{380} also has two peaks, one positive and one negative. The H₂O data show similar trends but with slightly different lifetimes <75 fs and 420 ± 90 fs. At the 95% confidence interval, we are unable to report a lower error bound on the fast lifetime in H₂O using GLA; therefore, only the upper limit on lifetime is reported. The shape of DAS_{380} suggests that population is directly exchanging from the positive going feature to the negative going feature. The negative going feature mirrors that from DAS_{80} and is also readily identifiable as the ground state.

In order to interpret DAS_{80} , one must consider possible mechanisms that might contribute two peaks to the spectrum. In an appropriate kinetic model with these DAS, the integrated rate equation for feature III must contain e^{-t/τ_1} with a positive leading coefficient. The simplest possible mechanism that includes this condition is a three-step sequential kinetic mechanism. In the case of a sequential mechanism, the integrated rate law for feature III is $S_{III}(\Delta t) = \frac{A_0}{\tau_2 - \tau_1} [\tau_1 e^{-t/\tau_1} - \tau_2 e^{-t/\tau_2}]$. Assuming these kinetics, an expression for the predicted DAS for each kinetic component can then be calculated.

For a kinetic model $I \xrightarrow{\tau_1} II \xrightarrow{\tau_2} III$ with the initial condition $I + II + III = 0$, expressions relating the DAS to the associated spectrum of the feature are given as follows:⁵²

$$DAS_{\tau_1} = S_I(eKE) - \frac{\tau_2}{\tau_2 - \tau_1} \sigma_{r,II} S_{II}(eKE) + \frac{\tau_1}{\tau_2 - \tau_1} \sigma_{r,III} S_{III}(eKE), \quad (3a)$$

$$DAS_{\tau_2} = \frac{\tau_2}{\tau_2 - \tau_1} \sigma_{r,II} S_{II}(eKE) - \frac{\tau_2}{\tau_2 - \tau_1} \sigma_{r,III} S_{III}(eKE). \quad (3b)$$

As shown in Eq. (3b), DAS_{τ_2} has a positive going component associated with feature II and a negative going component associated with feature III. Also, DAS_{τ_1} contains positive going components associated with features I and III. Using the equations above, spectra for features I and II can be generated by solving for S_{II} and S_{III} using the DAS from the fit and the known ground state. For both solvents, these spectra are shown in Figure 4. The extracted spectra for both solvents show very similar spectra. In D₂O, the ground state, feature III, is found to have a VBE of 3.38 ± 0.05 , and in H₂O, this feature has a VBE of 3.40 ± 0.05 eV. The VBE of Feature I is 2.1 ± 0.1 in D₂O and H₂O. Feature III shows little overlap with feature I. The VBE of feature II in both solvents is about 2.5 eV.

Because of the number of optimizable parameters inherent to GLA, the calculated error bounds on the kinetic components are quite large and are in fact too large to draw meaningful conclusions about isotope effects. In addition, Figs. 1(b) and 1(c) show that the photoelectron spectra in the eKE range of feature II shift toward lower energy on a time scale comparable to the lifetime of this feature, an effect that is not explicitly considered in GLA. We turn to a data analysis method with fewer fit parameters, integration of intensity in selected energy windows (lane integration), in order to directly compare the dynamics in specific spectral regions, and thus to assess the effect of isotopic substitution on the kinetics in the regions of interest. We improve upon the integrated intensity windows in our last presentation of the water data by using the associated spectra from GLA to select the three regions in Fig. 2(a) in which to fit the integrated intensity. The spectrally pure region of feature III, shown in green, lies below 1.2 eV. Feature I, the blue curve, does not overlap with feature II at kinetic energies greater than 3.0 eV. Feature II, the red curve, overlaps with both I and III, so the most reasonable place to integrate is the region of maximum intensity between 1.9 and 2.3 eV eKE. Based on these considerations, the blue, red, and green energy lanes in Figs. 1 and 2 are set at 2.8-3.5 eV, 1.9-2.3 eV, and 0.6-1.2 eV, so that the dominant contribution to the integrated signal in each lane comes from a single feature in Fig. 4.

Typical fit results from the integrated intensity in the energy regions of interest are shown in Fig. 2. Fit results from Fig. 2(a) (D₂O) yield time scales of 102 ± 8 fs for the blue

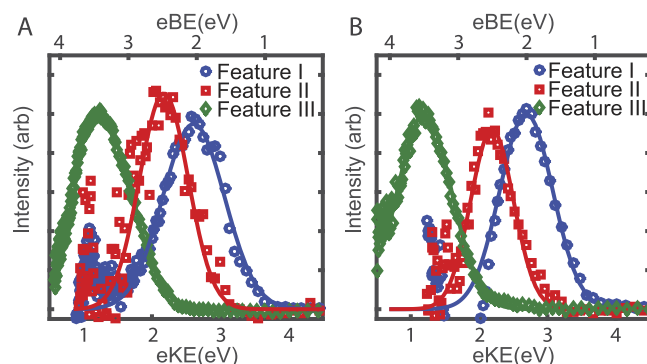


FIG. 4. Extracted spectra from Eqs. (3a) and (3b) for features I, II, and III in water (a) and D₂O (b).

TABLE I. Summary of fit parameters from GLA (columns 2 and 3) and lane integration (columns 4 and 5) $\pm 2\sigma$ interval.

Solvent	τ_1	τ_2	τ_1	τ_2
H ₂ O	<75 fs	420 \pm 90 fs	75 \pm 12 fs	400 \pm 70 fs
D ₂ O	80 \pm 30 fs	380 \pm 90 fs	102 \pm 8 fs	390 \pm 70 fs

lane, 390 \pm 70 fs for the red lane, and 410 \pm 60 fs for the green lane. Though the noise is equivalent for all time of flight bins, the magnitude of the noise becomes larger at low kinetic energy when scaled by the Jacobian transformation (Section II). As observed in Fig. 1(b), the time scales for the rise of the green curve and the decay of the red are the same within error. Further, integration in these energy lanes reproduces the lifetimes extracted from the GLA.

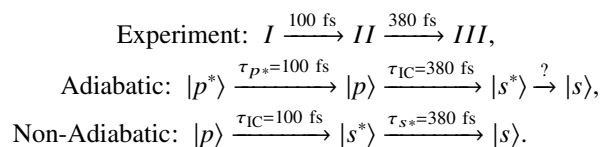
As shown in Fig. 2(b), the blue lane signal from H₂O decays more quickly than that from D₂O. A fit to the integrated intensity in this region yields a decay time of 75 \pm 12 fs for H₂O. The decay time for H₂O has a slightly larger error bound compared D₂O because, as in our previous work, the fast H₂O decay time is very near the limits of the time resolution of the experiment, in spite of improvements to the resolution. Using the time scales from lane integration, the isotope effect for this transition, $\tau(\text{D}_2\text{O})/\tau(\text{H}_2\text{O})$, is found to be 1.4 \pm 0.2. As shown in Fig. 2(c), a fit to the integrated red lane intensity in H₂O gives a decay time of 400 \pm 70 fs and yields no significant variation from the D₂O data.

In summary, from GLA we find two distinct kinetic components in each solvent whose associated spectra are well explained by a three-step sequential kinetic mechanism. In addition, the shapes of the associated spectra for features I, II, and III are similar in both solvents, and both solvents exhibit one decay time shorter than 100 fs and one of 380-400 fs. Using GLA to optimize energy regions for lane integration, we are able to report substantially narrower error bounds without imposing a bias on the selection of energy lanes. The fit decay times from both methods are summarized in Table I. Finally, we conclude that fastest decay (blue lane) in our spectra exhibits an isotope effect of 1.4 \pm 0.2, whereas the decay for the red lane does not show a measurable isotopic effect.

V. DISCUSSION

As detailed in Section I, the relaxation mechanism of the solvated electron after electronic excitation is expected to comprise three steps: relaxation on the excited state, internal conversion to the ground state, and solvent relaxation on the ground state. Three lifetimes were identified from prior work in water using transient absorption, <100 fs, 200-400 fs, and ~1.1 ps, and the assignment of the mechanism was narrowed to one of two possibilities.^{20,23,24} In the adiabatic mechanism, the fastest lifetime is assigned to τ_p , τ_{IC} is 200-400 fs, and τ_s is 1.1 ps. In the non-adiabatic mechanism, the <100 fs lifetime is assigned to τ_{IC} , and the ground state relaxes by a two-step mechanism.¹⁹ In our liquid jet measurements, we find two time constants of <100 fs and 400 fs that agree reasonably well with the faster two decays seen in TA. The two model

mechanisms are as follows:



As discussed in our previous work,^{51,52} much of the argument presented here hinges on the identification of which measured time constant corresponds with τ_{IC} . If the decay of feature I is from IC and the decay of feature II is from ground state relaxation subsequent to IC, then τ_{IC} is <100 fs and the relaxation mechanism is non-adiabatic. If the decay of feature I is from relaxation on the p -state and the decay of feature II is from IC from the relaxed p -state, then τ_{IC} is 400 fs and the mechanism is adiabatic. Our previous results on liquid jets of water and methanol were interpreted to favor the non-adiabatic mechanism. Here, new results including improved time resolution and data fitting routines along with new data for D₂O provide additional insight into the p -state relaxation dynamics.

Our previous arguments in favor of assigning feature I to IC apply here, as well. By comparing Figs. 1 and 4, the energy interval corresponding to Feature II has clear overlap with the high eKE edge of the ground state peak as would be expected from the unrelaxed ground state, i.e., the red lane in Fig. 1(a) looks like a vibrational hot band in photoelectron spectroscopy. Second, Fig. 4 shows that the maxima of features I and II are separated by 0.5 eV in both solvents. If this shift were due to relaxation on the p -state, it would imply that the p -state is stabilized by 0.5 eV prior to IC. However, all simulations of hydrated electron dynamics indicate that energy of the p -state remains relatively constant; instead, it is the s -state energy that is sensitive to solvent relaxation.^{12,27,35} Furthermore, as shown in Figs. 1(b), 1(c), and 2(d), the signal from 1.8 to 2.3 eV, corresponding to feature II, appears to shift as it decays. This trend is more apparent for D₂O than H₂O owing to the slower decay of feature I and is suggestive of relaxation as opposed to IC. Based on these observations, it appears reasonable to assign the 75 \pm 12 fs lifetime in water, 102 \pm 8 fs in D₂O, to internal conversion and conclude that the relaxation mechanism for both solvents is non-adiabatic. The 400 fs lifetime in both solvents is then assigned to solvent relaxation on the ground state. In recent results by Karashima *et al.*, photoelectron angular distributions (PADs) were measured in a similar three-pulse experiment on a liquid jet.⁵⁸ They find that the sub-100 fs lifetime is accompanied by a change in PAD, suggesting that this lifetime is indeed associated with a non-radiative electronic transition, consistent with its assignment to IC.

Based on this assignment, the isotope effect for IC is 1.4 \pm 0.2. This value lies within range of the isotope effects of 1.2-1.6 associated with the fastest decays measured in TA experiments.^{20,24,25} The lifetimes for solvent relaxation on the ground state do not show an isotope effect within error bars, but we cannot rule out a 10% effect as might be expected if solvent translational motion were the primary means of solvent relaxation.²⁶ While the observation of a clear isotope effect associated with Feature I might be interpreted as offering further support for its assignment to IC based

on comparison to early mixed quantum-classical molecular dynamics simulations,^{26,34} one must exercise caution in doing so because quantum decoherence effects can significantly reduce the calculated isotope effect for IC.^{36,42,70} We note, however, that the isotope effect measured here is very close to the IC isotope effect of 1.22 calculated by Prezhdo and Rossky⁴² when both quantum decoherence and quantized solvent vibrations are incorporated. The calculated IC time constants from Prezhdo and Rossky of 122 fs and 149 fs for H₂O and D₂O, respectively, are each within a factor of two of the experimental time constants found here.

Extrapolation of the τ_{IC} for water and deuterated water cluster anions of size 70–200 molecules yields an IC lifetime for water of 63 ± 6 and for D₂O 160 ± 18 fs, an isotope effect of 2.8 that is considerably larger than the value found here.⁴⁰ In that study, the choice to include only the larger solvent clusters into the fit was motivated by a discontinuity in cluster-dependent IC lifetimes around at $n = 70$. This discontinuity suggested a possible structural change after which larger clusters would become a better analog for bulk hydrated electrons.⁷¹ Including sizes 13–100 for water and sizes 25–50 in D₂O yields lifetimes of 54 ± 30 fs and 72 ± 22 fs for water and D₂O, respectively, an isotope effect of 1.2.³⁹ Hence, the fast lifetime for D₂O, 102 ± 8 fs, and the isotope effect measured here are in better agreement with extrapolated results which do not include large cluster sizes; the extrapolated IC lifetime for (H₂O)_n⁻ appears far less sensitive to the chosen size range. In experiments of (H₂O)_n⁻ cluster anions, Young *et al.*⁷² found a variation in τ_{IC} but not the detachment energy with clustering temperature in cluster anions, with faster IC times in warmer source conditions. It is possible that the (D₂O)_n⁻ clusters with $n > 70$ are colder than the smaller clusters, resulting in poorer agreement between the extrapolated IC lifetime with that of bulk D₂O. The considerably smaller discrepancy for H₂O may arise because D₂O cluster anions are generally expected to be less fluxional than (H₂O)_n⁻ clusters at the same temperature and may thus be more prone to forming structures in which the solvent-electron interaction differs from that in the bulk liquid.²⁶

VI. CONCLUSION

Time-resolved photoelectron spectroscopy measurements have been performed on solvated electrons in liquid jets of H₂O and D₂O. After excitation of the $s \rightarrow p$ absorption band, the relaxation dynamics of the excited electron are monitored as a function of pump-probe delay. The time-evolving spectra decay on two time scales: a sub-100 fs time scale that exhibits an isotope effect of 1.4 ± 0.2 and a time scale of ~ 400 fs that shows no measurable isotope effect. On the basis of the overall time evolution of the transients, the sub-100 fs decays are assigned to ps internal conversion and the slower time to relaxation subsequent to IC; the observed isotope effect is thus associated with IC. These assignments, which are consistent with past work on H₂O and methanol liquid jets, support the non-adiabatic model for relaxation of electronically excited hydrated electrons.

We hope that the results presented here motivate new theoretical treatments of time-resolved liquid jet photoelectron

spectroscopy, with particular focus on simulating how the relaxation dynamics of the hydrated electron map onto the photoelectron kinetic energy distribution. Such studies would be exceedingly useful in testing our interpretation of the time-resolved signals, particularly the assignment of the fastest dynamics to internal conversion.

ACKNOWLEDGMENTS

This work was funded by the National Science Foundation under the Grant No. CHE-1361412. Additional support is provided by the Air Force Office of Scientific Research under Grant No. 24086151-06 as part of the MURI topic “Time-Resolved Quantum Dynamics of Complex Systems.” H.L.W. is supported through the UC Berkeley Center for Solvation Studies, CALSOLV, in collaboration with Ruhr Explores Solvation, RESOLV, and funded by 28 Mio. EUR by the Deutsche Forschungsgemeinschaft (DFG). The authors thank Benjamin Schwartz at UCLA for helpful discussions regarding isotope effects. The data presented here are available on request sent to dneumark@berkeley.edu.

- ¹E. J. Hart and J. W. Boag, *J. Am. Chem. Soc.* **84**, 4090 (1962).
- ²B. Boudaïffa, P. Cloutier, D. Hunting, M. A. Huels, and L. Sanche, *Science* **287**, 1658 (2000).
- ³B. C. Garrett, D. A. Dixon, D. M. Camaioni, D. M. Chipman, M. A. Johnson, C. D. Jonah, G. A. Kimmel, J. H. Miller, T. N. Rescigno, P. J. Rossky, S. S. Xantheas, S. D. Colson, A. H. Laufer, D. Ray, P. F. Barbara, D. M. Bartels, K. H. Becker, K. H. Bowen, S. E. Bradforth, I. Carmichael, J. V. Coe, L. R. Corrales, J. P. Cowin, M. Dupuis, K. B. Eisenthal, J. A. Franz, M. S. Gutowski, K. D. Jordan, B. D. Kay, J. A. LaVerne, S. V. Lymar, T. E. Madey, C. W. McCurdy, D. Meisel, S. Mukamel, A. R. Nilsson, T. M. Orlando, N. G. Petrik, S. M. Pimblott, J. R. Rustad, G. K. Schenter, S. J. Singer, A. Tokmakoff, L.-S. Wang, and T. S. Zwier, *Chem. Rev.* **105**, 355 (2005).
- ⁴J. Gu, J. Leszczynski, and H. F. Schaefer, *Chem. Rev.* **112**, 5603 (2012).
- ⁵P. E. Mason, F. Uhlig, V. Vaněk, T. Buttersack, S. Bauerecker, and P. Jungwirth, *Nat. Chem.* **7**, 250 (2015).
- ⁶J. L. Ellis, D. D. Hickstein, W. Xiong, F. Dollar, B. B. Palm, K. E. Keister, K. M. Dorney, C. Ding, T. Fan, M. B. Wilker, K. J. Schnitzenbaumer, G. Dukovic, J. L. Jimenez, H. C. Kapteyn, and M. M. Murnane, *J. Phys. Chem. Lett.* **7**, 609 (2016).
- ⁷C.-R. Wang, J. Nguyen, and Q.-B. Lu, *J. Am. Chem. Soc.* **131**, 11320 (2009).
- ⁸L. Kevan, *Radiat. Phys. Chem.* **17**, 413 (1981).
- ⁹P. J. Rossky and J. Schnitker, *J. Phys. Chem.* **92**, 4277 (1988).
- ¹⁰H. F. Hameka, G. W. Robinson, and C. J. Marsden, *J. Phys. Chem.* **91**, 3150 (1987).
- ¹¹A. L. Sobolewski and W. Domcke, *Phys. Chem. Chem. Phys.* **9**, 3818 (2007).
- ¹²R. E. Larsen, W. J. Glover, and B. J. Schwartz, *Science* **329**, 65 (2010).
- ¹³F. Uhlig, O. Marsalek, and P. Jungwirth, *J. Phys. Chem. Lett.* **3**, 3071 (2012).
- ¹⁴M. Boero, M. Parrinello, K. Terakura, T. Ikeshoji, and C. C. Liew, *Phys. Rev. Lett.* **90**, 226403 (2003).
- ¹⁵J. M. Herbert and L. D. Jacobson, *Int. Rev. Phys. Chem.* **30**, 1 (2011).
- ¹⁶A. Migus, Y. Gauduel, J. Martin, and A. Antonetti, *Phys. Rev. Lett.* **58**, 1559 (1987).
- ¹⁷F. H. Long, X. L. Shi, H. Lu, and K. B. Eisenthal, *J. Phys. Chem.* **98**, 7252 (1994).
- ¹⁸X. Y. Chen and S. E. Bradforth, *Annu. Rev. Phys. Chem.* **59**, 203 (2008).
- ¹⁹L. Turi and P. J. Rossky, *Chem. Rev.* **112**, 5641 (2012).
- ²⁰K. Yokoyama, C. Silva, D. H. Son, P. K. Walhout, and P. F. Barbara, *J. Phys. Chem. A* **102**, 6957 (1998).
- ²¹C. Silva, P. K. Walhout, K. Yokoyama, and P. F. Barbara, *Phys. Rev. Lett.* **80**, 1086 (1998).
- ²²A. Baltuska, M. F. Emde, M. S. Pshenichnikov, and D. A. Wiersma, *J. Phys. Chem. A* **103**, 10065 (1999).
- ²³M. Assel, R. Laenen, and A. Laubereau, *Chem. Phys. Lett.* **317**, 13 (2000).
- ²⁴M. S. Pshenichnikov, A. Baltuska, and D. A. Wiersma, *Chem. Phys. Lett.* **389**, 171 (2004).

- ²⁵A. Thaller, R. Laenen, and A. Laubereau, *Chem. Phys. Lett.* **398**, 459 (2004).
- ²⁶B. J. Schwartz and P. J. Rossky, *J. Chem. Phys.* **105**, 6997 (1996).
- ²⁷B. J. Schwartz and P. J. Rossky, *J. Chem. Phys.* **101**, 6902 (1994).
- ²⁸D. Borgis, P. J. Rossky, and L. Turi, *J. Chem. Phys.* **125**, 064501 (2006).
- ²⁹D. Borgis, P. J. Rossky, and L. Turi, *J. Chem. Phys.* **127**, 174508 (2007).
- ³⁰A. Staib and D. Borgis, *J. Chem. Phys.* **103**, 2642 (1995).
- ³¹A. Hertwig, H. Hippler, A. N. Unterreiner, and P. Vohringer, *Ber. Bunsengesellschaft Phys. Chem.* **102**, 805 (1998).
- ³²T. W. Kee, D. H. Son, P. Kambhampati, and P. F. Barbara, *J. Phys. Chem. A* **105**, 8434 (2001).
- ³³J. Li, Z. Nie, Y. Y. Zheng, S. Dong, and Z.-H. Loh, *J. Phys. Chem. Lett.* **4**, 3698 (2013).
- ³⁴E. Neria and A. Nitzan, *J. Chem. Phys.* **99**, 1109 (1993).
- ³⁵R. E. Larsen, M. J. Bedard-Hearn, and B. J. Schwartz, *J. Phys. Chem. B* **110**, 20055 (2006).
- ³⁶B. J. Schwartz, E. R. Bittner, O. V. Prezhdo, and P. J. Rossky, *J. Chem. Phys.* **104**, 5942 (1996).
- ³⁷M. J. Tauber and R. A. Mathies, *J. Phys. Chem. A* **105**, 10952 (2001).
- ³⁸A. E. Bragg, J. R. R. Verlet, A. Kammrath, O. Cheshnovsky, and D. M. Neumark, *Science* **306**, 669 (2004).
- ³⁹A. E. Bragg, J. R. R. Verlet, A. Kammrath, O. Cheshnovsky, and D. M. Neumark, *J. Am. Chem. Soc.* **127**, 15283 (2005).
- ⁴⁰G. B. Griffin, R. M. Young, O. T. Ehrler, and D. M. Neumark, *J. Chem. Phys.* **131**, 194302 (2009).
- ⁴¹A. A. Zharikov and S. F. Fischer, *J. Chem. Phys.* **124**, 054506 (2006).
- ⁴²O. V. Prezhdo and P. J. Rossky, *J. Chem. Phys.* **107**, 5863 (1997).
- ⁴³C.-Y. Yang, K. F. Wong, M. S. Skaf, and P. J. Rossky, *J. Chem. Phys.* **114**, 3598 (2001).
- ⁴⁴J. M. Weber, J. Kim, E. A. Woronowicz, G. H. Weddle, I. Becker, O. Cheshnovsky, and M. A. Johnson, *Chem. Phys. Lett.* **339**, 337 (2001).
- ⁴⁵J. R. R. Verlet, A. E. Bragg, A. Kammrath, O. Cheshnovsky, and D. M. Neumark, *Science* **307**, 93 (2005).
- ⁴⁶A. T. Shreve, T. A. Yen, and D. M. Neumark, *Chem. Phys. Lett.* **493**, 216 (2010).
- ⁴⁷Y. Tang, Y.-I. Suzuki, H. Shen, K. Sekiguchi, N. Kurahashi, K. Nishizawa, P. Zuo, and T. Suzuki, *Chem. Phys. Lett.* **494**, 111 (2010).
- ⁴⁸A. Lübcke, F. Buchner, N. Heine, I. V. Hertel, and T. Schultz, *Phys. Chem. Chem. Phys.* **12**, 14629 (2010).
- ⁴⁹K. R. Siefertmann, Y. X. Liu, E. Lugovoy, O. Link, M. Faubel, U. Buck, B. Winter, and B. Abel, *Nat. Chem.* **2**, 274 (2010).
- ⁵⁰T. Horio, H. Shen, S. Adachi, and T. Suzuki, *Chem. Phys. Lett.* **535**, 12 (2012).
- ⁵¹M. H. Elkins, H. L. Williams, A. T. Shreve, and D. M. Neumark, *Science* **342**, 1496 (2013).
- ⁵²M. H. Elkins, H. L. Williams, and D. M. Neumark, *J. Chem. Phys.* **142**, 234501 (2015).
- ⁵³D. H. Paik, I.-R. Lee, D.-S. Yang, J. S. Baskin, and A. H. Zewail, *Science* **306**, 672 (2004).
- ⁵⁴O. T. Ehrler and D. M. Neumark, *Acc. Chem. Res.* **42**, 769 (2009).
- ⁵⁵B. Winter and M. Faubel, *Chem. Rev.* **106**, 1176 (2006).
- ⁵⁶Y.-I. Yamamoto, Y.-I. Suzuki, G. Tomasello, T. Horio, S. Karashima, R. Mitrc, and T. Suzuki, *Phys. Rev. Lett.* **112**, 187603 (2014).
- ⁵⁷S. Thürmer, R. Seidel, M. Faubel, W. Eberhardt, J. C. Hemminger, S. E. Bradforth, and B. Winter, *Phys. Rev. Lett.* **111**, 173005 (2013).
- ⁵⁸S. Karashima, Y.-I. Yamamoto, and T. Suzuki, *Phys. Rev. Lett.* **116**, 137601 (2016).
- ⁵⁹J. D. Smith, C. D. Cappa, W. S. Drisdell, R. C. Cohen, and R. J. Saykally, *J. Am. Chem. Soc.* **128**, 12892 (2006).
- ⁶⁰F. Buchner, A. Lübcke, N. Heine, and T. Schultz, *Rev. Sci. Instrum.* **81**, 113107 (2010).
- ⁶¹Y.-I. Suzuki, K. Nishizawa, N. Kurahashi, and T. Suzuki, *Phys. Rev. E* **90**, 010302 (2014).
- ⁶²P. Kruit and F. H. Read, *J. Phys. E* **16**, 313 (1983).
- ⁶³A. T. Shreve, M. H. Elkins, and D. M. Neumark, *Chem. Sci.* **4**, 1633 (2013).
- ⁶⁴J. R. Knutson, D. G. Walbridge, and L. Brand, *Biochemistry* **21**, 4671 (1982).
- ⁶⁵I. H. M. van Stokkum, D. S. Larsen, and R. van Grondelle, *Biochim. Biophys. Acta* **1657**, 82 (2004).
- ⁶⁶P. Fita, E. Luzina, T. Dziembowska, C. Radzewicz, and A. Grabowska, *J. Chem. Phys.* **125**, 184508 (2006).
- ⁶⁷Y.-I. Suzuki, H. Shen, Y. Tang, N. Kurahashi, K. Sekiguchi, T. Mizuno, and T. Suzuki, *Chem. Sci.* **2**, 1094 (2011).
- ⁶⁸A. S. Chatterley, C. W. West, G. M. Roberts, V. G. Stavros, and J. R. R. Verlet, *J. Phys. Chem. Lett.* **5**, 843 (2014).
- ⁶⁹H. Marciniak and S. Lochbrunner, *Chem. Phys. Lett.* **609**, 184 (2014).
- ⁷⁰O. V. Prezhdo and P. J. Rossky, *Phys. Rev. Lett.* **81**, 5294 (1998).
- ⁷¹N. I. Hammer, J.-W. Shin, J. M. Headrick, E. G. Diken, J. R. Roscioli, G. H. Weddle, and M. A. Johnson, *Science* **306**, 675 (2004).
- ⁷²R. M. Young, M. A. Yandell, S. B. King, and D. M. Neumark, *J. Chem. Phys.* **136**, 094304 (2012).